Journal of Mines, Metals and Fuels, *71(12C) : 07-15; 2023. DOI: 10.18311/jmmf/2023/47271*

Print ISSN : 0022-2755

Journal of Mines, Metals and Fuels

Contents available at: *www.informaticsjournals.com/index.php/jmmf*

Metal Detection by the Estimation of HOMO-LUMO and Global Reactivity Descriptors of 1-Methyl-1H-Imidazole Substituted Coumarin

A. Anthony Seleen[1], T. P. Jyothi[2], R. Shwetha[3], Lohit Naik[4], Yin Yao[5], Yury Kapelyushin[6], Charles Mbohwa[7] and U. Mahaboob Pasha[7,8*]

[1]Government First Grade College, Kolar Gold Fields - 563122, Karnataka, India
[2]Government First Grade College, K.R. Puram, Bangalore - 560036, Karnataka, India
[3]Department of Physics, MES College of Science, Commerce and Arts, Bangalore -560003, Karnataka, India
[4]Christ University, Bangalore - 560026, Karnataka, India
[5]Electron Microscope Unit, Mark Wainwright Analytical Centre, UNSW Sydney, Sydney, New South Wales - 2052, Australia
[6]Faculty of Materials Science and Metallurgy Engineering, South Ural State University (National Research University), Prospekt Lenina, 76, Chelyabinsk, Chelyabinsk Oblast-454080, Russia
[7]College of Science Engineering and Technology, University of South Africa, Pretoria, South Africa
[8]Presidency University, Bangalore - 560064, Karnataka, India; mahaboobpasha@presidencyuniversity.in*

Abstract

In this study, the photophysical properties of the compound 4-((2-(1H-benzo[d]imidazol-1-yl)-1-(2-oxo-2H-chromen-3-yl) ethoxy) methyl)-6-methyl-2H-chromen-2-one (2HBXO) using Density Functional Theory (DFT) with the B3LYP functional and the 6-311G basis set was investigated. The optimised molecular geometry, Mulliken charge distribution and the energy gap between the Highest Occupied Molecular Orbital (HOMO) and the Lowest Unoccupied Molecular Orbital (LUMO) were examined in different solvent environments. This enabled us to calculate solvation energy, ionisation potential, electron affinity, chemical hardness, electronegativity, electron chemical potential and global electrophilicity. The total electron density and molecular electrostatic potential distributions were also analysed to gain insights into the potential distribution across the molecule. Based on these findings, this coumarin derivative's electronic and spectroscopic characteristics. The presence of electronegative sites in 2HBXO suggests its potential application as a sensor for detecting metal ions.

Keywords: Coumarin Derivative, FMO, MESP, Mulliken, UV-Vis

1.0 Introduction

Coumarins, a class of oxygen-containing heterocyclic compounds, have gained significant attention in various scientific fields due to their unique structural and optoelectronic properties. These compounds are categorised as lactones containing a benzopyrone skeletal framework, which is formed by the fusion of benzene and pyrone rings at the second position of the pyrone carbonyl[1]. Naturally occurring coumarins are widely isolated from plants, making them one of the major classes of organic compounds with diverse functionalities.

**Author for correspondence*

Moreover, the synthesis of novel synthetic coumarins and their derivatives with various functional groups is well-established, allowing researchers to tailor their properties for specific applications. Coumarins exhibit remarkable photophysical and spectroscopic properties, largely attributed to their π-conjugated structures[2]. These properties have paved the way for their extensive use in various optoelectronic applications, including Organic Light-Emitting Diodes (OLEDs), electroluminescent devices, fluorescent materials, nonlinear optical materials and laser dyes. The ability to modify the coumarin core by attaching different substituents allows for fine-tuning of their optoelectronic properties, making them highly versatile for different technological applications. For instance, coumarins have been utilised as organic sensitisers in high-efficiency Dye-Sensitised Solar Cells (DSSCs), where their strong light absorption and efficient charge transfer capabilities are crucial for improving device performance[3-5].

In addition to their optoelectronic applications, coumarins have also found significant roles in biological systems. Their inherent fluorescence properties make them ideal candidates for use as fluorescent probes and sensors for detecting metal ions and other biological molecules. Furthermore, coumarins have been explored as pharmaceutical agents due to their diverse biological activities, including anti-inflammatory, anticoagulant, antimicrobial and anticancer properties. The ability to modify the chemical structure of coumarins allows for the development of derivatives with enhanced biological activity, thus expanding their potential therapeutic applications[6-9].

Understanding the structure-property relationships of coumarins is essential for advancing their use in both optoelectronic and biological applications. Studies have shown that the introduction of various substituents can significantly influence the Intramolecular Charge Transfer (ICT) processes, leading to enhanced wavelength tuning and improved photophysical performance. For example, fluorinated coumarins have been shown to absorb UV-visible light at specific wavelengths and exhibit fluorescence emission, making them suitable for use in optical devices and as biological imaging agents[10-13]. Overall, the versatility of coumarins in optoelectronic and biological applications is a testament to their unique structural and photophysical properties. As research in this field continues to evolve, coumarins and their derivatives are expected to play an increasingly important role in the development of advanced materials and technologies. Given the above, 1-methyl-1H-imidazole substituted coumarin derivatives represent a promising class of compounds with multifaceted pharmacological and optoelectronic attributes. In light of the above discussion, the present work focuses on the compound, examining its photophysical and chemical properties through Density Functional Theory (DFT) analysis[14-15].

2.0 Analysis of Density Functional Theory

The 1-methyl-1H-imidazole substituted coumarin derivatives, namely 4-((2-(1H-benzo[d]imidazol-1-yl)-1-(2-oxo-2H-chromen-3-yl)ethoxy)methyl)-6-methyl-2H-chromen-2-one (2HBXO) is selected from the literature[16]. The molecular structure of the 2HBXO is given in Figure 1.

The structural and theoretical analyses of 2HBXO were conducted using GaussView 5.0 and Gaussian-09 W software packages[17]. The optimisation of 2HBXO geometry was initially performed via DFT employing the B3LYP functional and 6-311G basis set. DFT with the B3LYP functional and the 6-311G basis set is a widely used approach for studying the electronic structure of molecules. In this study, we applied DFT to investigate the photophysical and electronic properties of the coumarin derivative 2HBXO. Key parameters such as optimised geometry, HOMO-LUMO energy gap, and electron density distribution were analysed to understand its electronic behaviour and potential for metal ion sensing.

The energy levels of the HOMO and LUMO were examined across different mediums, allowing for the assessment of key molecular properties such as ionisation ability, electron affinity, chemical hardness and electrophilic index. Additionally, DFT was employed to analyse the Total Electron Density (TED) surface mapping, Electrostatic Potential (ESP), Molecular



Figure 1. Molecular structure of the 2HBXO molecule.

Electrostatic Potential (MEP) and contour mapping of 2HBXO in both vacuum and solvent mediums, offering insights into its molecular interactions.

3.0 Results and Discussions

3.1 Structure and Geometric Properties

The structural design of 2HBXO was initially generated in GaussView-5 and subsequently optimised using Gaussian 09 software. The optimisation process, conducted with the "opt" keyword, utilised the B3LYP functional and the 6-311G basis set[18]. Starting from standard parameters, the Gaussian program iteratively minimised the geometry to identify the configuration with the lowest energy, resembling the molecular structure at its energy minimum. The resulting optimised molecular geometries of 2HBXO are depicted in Figure 2, providing a visual representation of the molecule's conformational characteristics.

The structural analysis of the molecule reveals detailed insights into its bond lengths, bond angles and dihedral angles, as presented in Table 1. The optimised geometry of the molecule 4-((2-(1H-benzo[d] imidazol-1-yl)-1-(2-oxo-2H-chromen-3-yl)ethoxy) methyl)-6-methyl-2H-chromen-2-one provides insights into its structural stability and flexibility, essential for understanding its potential applications. The bond lengths for the carbonyl groups (C1-O12 at 1.233 Å and C26-O36 at 1.233 Å) indicate strong double-bond characteristics, suggesting substantial conjugation within the molecule. These short bond lengths reflect the rigidity and planarity of the molecule's conjugated systems, which stabilise the structure through resonance and electronic delocalisation. In contrast, the longer ether bonds (C1-O13 at 1.419 Å and C26-O37 at 1.427 Å) are indicative of single-bond character, introducing some flexibility into the molecule. This flexibility allows the molecule to adopt various conformations, which can be crucial for interactions with external agents, such as metal ions. The bond angles around the carbonyl and ether groups, such as C1-O13-C5 (121.81°) and O12-C1-C2 (126.89°), are close to typical values for sp^2 hybridized carbons, indicating a planar structure conducive to effective π-electron delocalisation. This planarity enhances the molecule's stability and contributes to its electronic properties by allowing efficient overlap of p-orbitals. The dihedral angles provide insights into the molecule's torsional strain and flexibility. For instance, H17-C16-O19-C20 (59.71°) and C16-O19-C20-C25 (58.48°) reflect significant twisting or non-planarity between different groups attached to the core, which can introduce some torsional strain. However, this strain also contributes to the molecule's ability to adapt its conformation, which could be beneficial for its function as a sensor. In contrast, dihedral angles such as H56-C55-C8-C9 (150.66°) and H40-C38-N54-C41 (172.92°) suggest near-planar arrangements in parts of the molecule, enhancing conjugation and stability in these regions. The molecule exhibits a balance between rigidity and flexibility. The rigid, conjugated regions provide structural stability and enhance electronic properties through delocalisation, while the flexible, single-bond areas allow the molecule to adjust its conformation. This dual nature is advantageous for applications like metal ion sensing, where the molecule needs to maintain a stable electronic structure while being flexible enough to interact with target ions or molecules. The optimised geometry shows that the molecule combines a stable conjugated system with flexible linkages, allowing it to potentially adapt its structure for various functional applications while maintaining overall stability[19].

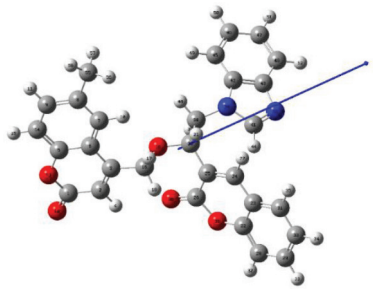


Figure 2. Optimised molecular geometry of the 2HBXO molecule.

The Mulliken atomic charge distributions[20-21] of each atomic site in 2HBXO were investigated using DFT with the B3LYP/6-311G method in three different environments, vacuum, hexene, and DMSO which are useful for various atomic and molecular fields. Table 2 presents the Mulliken charge distribution of each atom in 2HBXO different mediums, highlighting the solvent influences. Figures 3 and 4 graphically illustrate the variation in charge distribution across molecules. Notably, the atomic charges exhibited an increase with the polarity of the solvent, with the highest values observed in DMSO. In a vacuum, specific carbon and nitrogen atoms showed negative charges, suggesting donor characteristics, while

Table 1. Estimation of bond length (Å), bond angle (°) and dihedral angle of HCE using DFT/B3LYP/6-311G.

Atoms	Bond Length (Å)	Atoms	Bond Angle (°)	Atoms	Dihedral Angle (°)
C1-O12	1.233	C1-O13-C5	121.81	H17-C16-O19-C20	59.71
C1-O13	1.419	O13-C1-O12	118.33	H56-C55-C8-C9	150.66
C1-C2	1.459	O12-C1-C2	126.89	H40-C38-N54-C41	172.92
C2-C3	1.360	C8-C55-H58	111.57	H58-C55-C8-C9	30.22
C3-C6	1.458	C3-C16-O19	107.15	C16-O19-C20-C25	58.48
C6-C7	1.412	C16-O19-C20	114.37	O19-C20-C30-H40	51.90
C7-C8	1.406	O19-C20-C25	114.05		
C8-C55	1.513	C25-C20-C38	116.62		
C55-H56	1.094	H40-C38-H39	107.91		
C3-C16	1.507	C20-C38-N54	115.35		
C16-O19	1.457	N54-C41-N53	113.31		
O19-C20	1.439	C41-N53-C41	105.92		
C20-C38	1.546	N53-C43-C42	109.82		
C38-N54	1.482	C43-C42-N54	105.67		
N54-C41	1.418	O36-C26-O37	118.29		
C41-N53	1.308	C26-O37-C22	123.38		
N53-C43	1.417				
C43-C42	1.412				
C42-N54	1.424				
C20-C25	1.516				
C26-O36	1.233				
C26-O37	1.427				
C25-C26	1.456				
C41-H44	1.075				

others acted as acceptors. Transitioning to hexene, a slight increase in hydrogen and carbon atom charges was noted, along with a noticeable rise in the charge of nitrogen atoms compared to the vacuum. In DMSO, an overall elevation in atomic charges was observed across all atoms, indicating enhanced solvation effects. Additionally, a marginal increase in oxygen atom charge was evident with the shift from vacuum to hexene and further to DMSO. These insights into atomic charge distribution provide valuable information for understanding molecular interactions and the influence of solvents on 2HBXO's chemical behaviour.

The Mulliken atomic charges calculated for your organic molecule in vacuum, hexene and DMSO reflect how electron density shifts across different environments. In a vacuum, the charges serve as a baseline, showing the molecule's natural electron distribution without external influence. For example, atom 1C has a charge of +0.507, atom 2C has a charge of -0.194, and atom 12O carries a significant negative charge of -0.417. Hydrogen atoms, like 4H, have small positive charges, such as +0.197. When the molecule is placed in hexene, a non-polar solvent, there are subtle shifts in electron density. The charge on 1C increases to +0.628, and the charge on 2C becomes less negative at -0.073, while the charge on 12O decreases in magnitude to -0.296. These modest changes indicate that hexene, being non-polar, causes only slight alterations in the electron distribution, which can still influence the molecule's reactivity in non-polar environments.

In contrast, DMSO, a polar solvent, induces more substantial shifts in Mulliken charges. For instance, the charge on 1C further increases to +0.683, and 2C's charge shifts to -0.018, becoming nearly neutral. The negative charge on 12O decreases further to -0.241. This behaviour

reflects DMSO's strong interaction with both positive and negative regions of the molecule, stabilising these charges. As a result, positive charges become more positive, and negative charges become less negative, leading to a more uniform charge distribution. This stabilisation effect in DMSO enhances the molecule's solubility in polar environments and affects its reactivity, making it more stable and less reactive compared to non-polar environments. Understanding these shifts is crucial for predicting the molecule's behaviour in different solvents, with significant implications for applications in drug design and chemical synthesis, where solvent choice can optimise reaction conditions and outcomes.

3.2 Frontier Molecular Orbitals (FMO) and Quantum Chemical Simulation

The FMOs are instrumental in understanding the electron transfer between donor and acceptor groups within a π-conjugated system. The HOMO is associated with the electron-donating capacity of the molecule and correlates with its ionisation potential, while the LUMO relates to the molecule's electron-accepting ability and its electron affinity. Analysing the FMO plots provides deeper insights into the chemical structure and reactivity of the compound. In this study, HOMO, HOMO-1 and HOMO-2 are identified as orbitals with π-bonding symmetry, whereas LUMO, LUMO+1 and LUMO+2 exhibit π* antibonding symmetry. Figure 5 illustrates a 3D representation of these frontier orbitals in different media using DFT with the B3LYP functional and 6-311G basis set. In this visualisation, the greenish areas represent positive regions, while the reddish areas indicate negative regions of the molecular orbitals.



Figure 3. Mulliken charge distribution on the 2HBXO molecule.

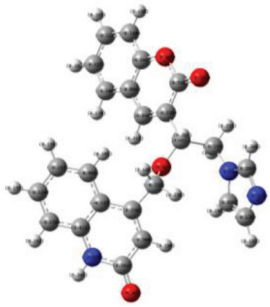


Figure 4. A statistical representation of Mulliken charge distribution on the 2HBXO molecule in the gas phase.

The energy gap (DE) between the HOMO and LUMO has been evaluated using the equation provided, with the following results: in DMSO, the largest energy gap of 4.205 eV was observed; the gap between HOMO-1 and LUMO+1 is 4.324 eV, and between HOMO+2 and LUMO-2, it is 6.068 eV. These findings highlight the varying electronic properties of the molecule in different environments.

The global electrochemical reactivity descriptors for the organic molecule 2HBOX are presented in Table 3. The energy of the highest occupied molecular orbital (E_{HOMO}) is -6.212 eV and the energy of the lowest unoccupied molecular orbital (E_{LUMO}) is -2.653 eV. The energy gap (ΔE), calculated as the difference between EHOMO and ELUMO, is 3.559 eV. A smaller ΔE indicates higher chemical reactivity and lower stability, suggesting that this molecule has moderate reactivity and stability. The Ionisation Potential (IP) is equal to the magnitude of EHOMO, which is 6.212 eV, and the Electron Affinity (EA) is equal to the magnitude of ELUMO, which is 2.653 eV. These values suggest the molecule's tendency to donate or accept electrons in chemical reactions.

The chemical hardness (η) is calculated as half of the ΔE, yielding a value of 1.780 eV, indicating the resistance to charge transfer within the molecule. The electronegativity (χ), calculated as the negative average of EHOMO and ELUMO, is 4.433 eV, reflecting the molecule's ability to attract electrons. The chemical potential (μ), which is the negative of electronegativity, is -4.433 eV, representing the escaping tendency of electrons from the molecule. The softness (s), the inverse of chemical hardness, is 0.281 eV^{-1}, indicating moderate reactivity. The electrophilicity index (ω) is 5.520 eV, suggesting a strong tendency to accept electrons. Overall, these descriptors suggest that the molecule has moderate reactivity and stability, with a significant tendency to participate in electron-accepting reactions.

Table 2. Mulliken atomic charges by DFT/B3LYP/6-311G in vacuum and solvent medium

Atom Label	Vacuum	Hexene	DMSO
1C	0.507	0.628	0.683
2C	-0.194	-0.073	-0.018
3C	0.128	0.249	0.304
4H	0.197	0.318	0.373
5C	0.280	0.401	0.456
6C	0.078	0.199	0.254
7C	-0.207	-0.086	-0.031
8C	0.098	0.219	0.274
9C	-0.156	-0.035	0.020
10H	0.134	0.255	0.310
11H	0.131	0.252	0.307
12O	-0.417	-0.296	-0.241
13O	-0.530	-0.409	-0.354
14C	-0.161	-0.040	0.015
15H	0.148	0.269	0.324
16C	-0.080	0.041	0.096
17H	0.128	0.249	0.304
18H	0.156	0.277	0.332
19O	-0.489	-0.368	-0.313
20C	0.091	0.212	0.267
21H	0.143	0.264	0.319
22C	0.288	0.409	0.464
23C	0.140	0.261	0.316
24C	-0.287	-0.166	-0.111
25C	-0.013	0.108	0.163
26C	0.514	0.635	0.690
27H	0.206	0.327	0.382
28C	-0.159	-0.038	0.017
29C	-0.105	0.016	0.071
30C	-0.121	0.000	0.055
31C	-0.180	-0.059	-0.004
32H	0.161	0.282	0.337
33H	0.148	0.269	0.324
34H	0.143	0.264	0.319
35H	0.151	0.272	0.327
36O	-0.397	-0.276	-0.221
37O	-0.519	-0.398	-0.343
38C	-0.130	-0.009	0.046
39H	0.189	0.310	0.365
40H	0.175	0.296	0.351
41C	0.227	0.348	0.403
42C	0.200	0.321	0.376

Table 2. Continued...

Atom Label	Vacuum	Hexene	DMSO
43C	0.061	0.182	0.237
44H	0.196	0.317	0.372
45C	-0.083	0.038	0.093
46C	-0.138	-0.017	0.038
47C	-0.139	-0.018	0.037
48C	-0.078	0.043	0.098
49H	0.140	0.261	0.316
50H	0.132	0.253	0.308
51H	0.130	0.251	0.306
52H	0.148	0.269	0.324
53H	-0.408	-0.287	-0.232
54H	-0.567	-0.446	-0.391
55C	-0.475	-0.354	-0.299
56H	0.146	0.267	0.322
57H	0.165	0.286	0.341
58H	0.153	0.274	0.329

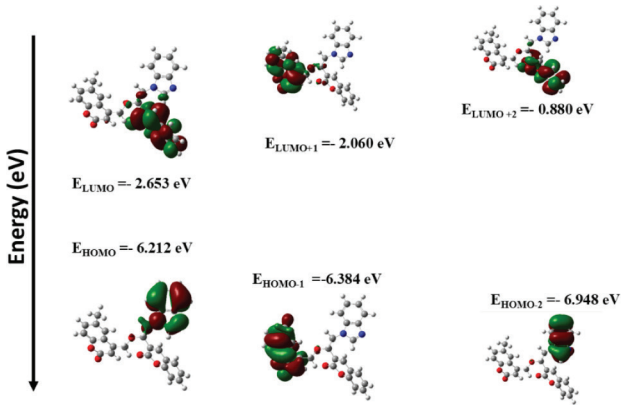


Figure 5. 3D representation of frontier molecular orbital of 2HBXO in DMSO using the DFT method.

3.3 Electrostatic Potential (ESP), Total Electron Density (TED) and Molecular Electrostatic Potential (MESP) Studies

Three-dimensional mappings of electrostatic potential, total electron density and molecular electrostatic potential were generated using DFT theory with the B3LYP functional and 6-311G basic set. These mappings of 2HBXO structure were analysed through surface contouring in Gaussian-09W. The ESP, TED and MESP[23-24] of 2HBXO are shown in Figure 6 to Figure 8.

Table 3. Global electrochemical reactivity descriptor parameter of 2HBOX

E_{HOMO} (eV)	E_{LUMO} (eV)	ΔE (eV)	IP (eV)	EA (eV)	h (eV)	c (eV)	μ (eV)	s (eV^{-1})	ω (eV)
-6.212	-2.653	3.559	6.212	2.653	1.780	4.433	-4.433	0.281	5.520

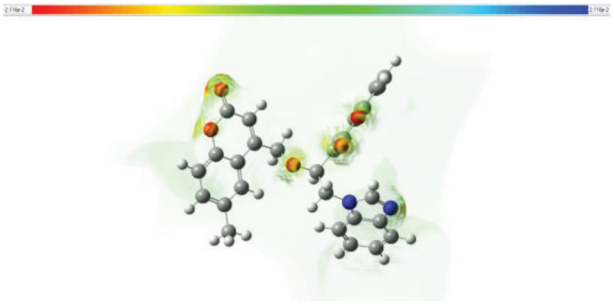


Figure 6. Electrostatic potential mapping of 2HBXO molecule in vacuum.



Figure 7. Total electron density mapping of 2HBXO molecule in vacuum.

The ESP illustrates the interaction energy between the molecule's electrons and point positive charges near nuclei. Figure 6 displays the ESP mapping of the 2HBXO molecule, indicating energy ranging from $-2.116x10^{-2}$ eV to $2.116x10^{-2}$ eV in vacuum. Notably, sites O30 and O31 exhibit the most negative potential values of -0.312 eV and -0.303 eV, respectively, in vacuum and these areas are highlighted in red. Additionally, the region encompassing 27N and 13N shows, the potential values of 0.121 eV and 0.111 eV (yellow) in vacuum. The TED Electron density mapping is used in analysing the molecule's shape, charge, and delocalisation, offering insights into its chemical reactivity. Figure 7 illustrates the TED mapping of 2HBXO in a vacuum, indicating electron densities of ± $4.065x10^{-4}$ hartrees in a vacuum. The electron density shows, a uniform distribution across the molecule's surface. These results help in understanding various properties of a system, such as chemical bonding, interactions and other important electronic properties. Figure 8 presents the MESP mapping of 2HBXO in vacuum and DMSO, displaying contour values ranging from -6.807 eV to 6.807 eV in vacuum. The red regions, primarily surrounding 12O, 13O, 37O and 36O, signify lower energy levels, making these atoms susceptible to nucleophilic attacks as electron acceptors. Conversely, the 1-methyl-1H-imidazole group attached to carbon atom 20C, 49N displays maximum positive charge (blue region), rendering them susceptible to electrophilic attacks as electron donors. Yellow colour around 54N and 53N represents nucleophilic sites. The neutral (green) region is widespread across the molecule, particularly

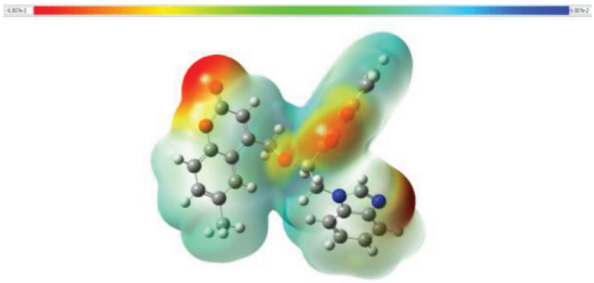


Figure 8. Molecular electrostatic potential mapping of 2HBXO molecule in vacuum.

on benzene ring structures and certain carbon atoms. Positive charge (light blue) is observed at the position of hydrogen indicating its role as an electron-donator[24].

4.0 Conclusion

The comprehensive structural, electrostatic and quantum chemical analysis of the 2HBXO reveals a balanced interaction between rigidity and flexibility, which is crucial for its potential applications in sensing and molecular interactions. The 2HBXO moderate energy gap and chemical descriptors suggest it has a stable electronic structure with a significant capacity for electron acceptance. The detailed analysis of bond lengths, angles and dihedral angles indicates a structure that is both stable and adaptable, capable of efficient π-electron delocalisation while maintaining sufficient flexibility for interaction with external agents. Additionally, the shifts in Mulliken atomic charges across different solvents highlight the molecule's adaptability and solvation effects,

which are essential for understanding its behaviour in various environments. The mapping of electrostatic potential, electron density and molecular electrostatic potential further corroborates the molecule's ability to engage in nucleophilic and electrophilic interactions, underscoring its potential utility in applications such as metal ion sensing and drug design. Overall, the molecule exhibits a well-balanced structure that combines stability with reactivity, making it a promising candidate for further exploration in the chemical and pharmaceutical fields.

5.0 References

1. Pratap R, Ram VJ. Natural and synthetic chromenes, fused chromenes, and versatility of dihydrobenzo[h]chromenes in organic synthesis. Chem Rev. 2014; 114(20):10476-526. https://doi.org/10.1021/cr500075s
2. Paramasivam M, Kanvah S. Rational tuning of AIEE active coumarin based α-cyano stilbenes toward far-red/NIR region using different π-spacer and acceptor units. J Phys Chem C. 2016; 120(20):10757-69. https://doi.org/10.1021/acs.jpcc.6b01334
3. Parola S, Julián-López B, Carlos LD, Sanchez C. Optical properties of hybrid organic-inorganic materials and their applications. Adv Funct Mater. 2016; 26(36):6506-44. https://doi.org/10.1002/adfm.201602730
4. Gangadhar PS, Reddy G, Prasanthkumar S, Giribabu L. Phenothiazine functional materials for organic optoelectronic applications. Phys Chem Phys. 2021; 23(28):14969-96. https://doi.org/10.1039/D1CP01185E
5. Dey A, Singh A, Das D, Iyer PK. Organic semiconductors: A new future of nanodevices and applications. Thin Film Struct Energy Appl. 2015; 97-128. https://doi.org/10.1007/978-3-319-14774-1_4
6. Sharifi-Rad J, Cruz-Martins N, López-Jornet P, Lopez EPF, Harun N, Yeskaliyeva B, *et al*. Natural coumarins: Exploring the pharmacological complexity and underlying molecular mechanisms. Oxid Med Cell Longev. 2021; 2021(1):6492346. https://doi.org/10.1155/2021/6492346
7. Wu L, Wang X, Xu W, Farzaneh F, Xu R. The structure and pharmacological functions of coumarins and their derivatives. Curr Med Chem. 2009; 16(32):4236-60. https://doi.org/10.2174/092986709789578187
8. Kostova I. Synthetic and natural coumarins as cytotoxic agents. Curr Med Chem Anticancer Agents. 2005; 5(1):29-46. https://doi.org/10.2174/1568011053352550
9. El-adly A, Shabana I. Antimicrobial activity of green silver nanoparticles against fluconazole-resistant *Candida albicans* in animal model. Egypt J Bot. 2018; 58(1):119-32. https://doi.org/10.21608/ejbo.2018.1292.1110
10. Cheke RS, Patel HM, Patil VM, Ansari IA, Ambhore JP, Shinde SD, *et al*. Molecular insights into coumarin analogues as antimicrobial agents: recent developments in drug discovery. Antibiotics. 2022; 11(5):566. https://doi.org/10.3390/antibiotics11050566
11. Kashyap PL, Xiang X, Heiden P. Chitosan nanoparticle based delivery systems for sustainable agriculture. Int J Biol Macromol. 2015; 77:36-51. https://doi.org/10.1016/j.ijbiomac.2015.02.039
12. Gedeck P, Kramer C, Ertl P. Computational analysis of structure-activity relationships. Prog Med Chem. 2010; 49:113-60. https://doi.org/10.1016/S0079-6468(10)49004-9
13. Piir G, Kahn I, García-Sosa AT, Sild S, Ahte P, Maran U. Best practices for QSAR model reporting: physical and chemical properties, ecotoxicity, environmental fate, human health, and toxicokinetics endpoints. Environ Health Perspect. 2018; 126(12):126001. https://doi.org/10.1289/EHP3264
14. Stefanachi A, Leonetti F, Pisani L, Catto M, Carotti A. Coumarin: A natural, privileged and versatile scaffold for bioactive compounds. Molecules. 2018; 23(2):250. https://doi.org/10.3390/molecules23020250
15. Taboureau O, Baell JB, Fernández-Recio J, Villoutreix BO. Established and emerging trends in computational drug discovery in the structural genomics era. Chem Biol. 2012; 19(1):29-41. https://doi.org/10.1016/j.chembiol.2011.12.007
16. Savanur HM, Pawashe GM, Kim KM, Kalkhambkar RG. Synthesis and molecular modelling studies of coumarin- and 1-aza-coumarin-linked miconazole analogues and their antifungal activity. ChemSelect. 2018; 3(33):9648-53. https://doi.org/10.1002/slct.201801408
17. Frisch MJ, Trucks GW, Schlegel HB, Scuseria GE, Robb MA, Cheeseman JR, *et al*. Gaussian-09, Revision B.01. Wallingford (CT): Gaussian, Inc.; 2010.
18. Raghavachari K. Density-functional thermochemistry. III. The role of exact exchange. J Chem Phys. 2000; 98:135. https://doi.org/10.1007/978-3-662-10421-7_60
19. Shirley WA, Hoffmann R, Mastryukov VS. An approach to understanding bond length/bond angle relationships. J Phys Chem. 1995; 99(12):4025-33. https://doi.org/10.1021/j100012a024
20. Tsuzuki S, Uchimaru T, Tanabe K, Yliniemela A. Comparison of atomic charge distributions obtained from different procedures: basis set and electron correlation effects. J Mol Struct Theochem. 1996; 365(2-3):81-8. https://doi.org/10.1016/0166-1280(96)04500-9
21. Petrushenko IK. Physical adsorption of N-containing heterocycles on hexagonal boron nitride: DFT-D3 study. J Nano Electron Phys. 2018; 10(2):1-9. https://doi.org/10.21272/jnep.10(2).02010

22. Zara Z, Iqbal J, Ayub K, Irfan M, Mahmood A, Khera RA, *et al*. A comparative study of DFT calculated and experimental UV/visible spectra for thirty carboline and carbazole based compounds. J Mol Struct. 2017; 1149:282-98. https://doi.org/10.1016/j.molstruc.2017.07.093
23. Nogueira JJ, González L. Computational photophysics in the presence of an environment. Annu Rev Phys Chem. 2018; 69:473-97. https://doi.org/10.1146/annurev-physchem-050317-021013
24. Tichnell CR, Shultz DA, Popescu CV, Sokirniy I, Boyle PD. Synthesis, characterization, and photophysical studies of an iron (III) catecholate-nitronylnitroxide spin-crossover complex. Inorg Chem. 2015; 54(9):4466-74. https://doi.org/10.1021/acs.inorgchem.5b00298